



Electronic inhomogeneity and band structure in superstructural CuO_2 planes of infinite-layer $\text{Sr}_{0.94}\text{La}_{0.06}\text{CuO}_{2+y}$ films

Rui-Feng Wang,¹ Jiaqi Guan,¹ Yan-Ling Xiong,¹ Xue-Feng Zhang,² Jia-Qi Fan²,,² Jing Zhu,² Can-Li Song^{1,3,*},,^{1,3,*}
Xu-Cun Ma,^{1,3,†} and Qi-Kun Xue^{1,3,4}

¹State Key Laboratory of Low-Dimensional Quantum Physics, Department of Physics, Tsinghua University, Beijing 100084, China

²Institute of Physics, National Center for Electron Microscopy in Beijing, School of Materials Science and Engineering, Tsinghua University, Beijing 100084, China

³Frontier Science Center for Quantum Information, Beijing 100084, China

⁴Beijing Academy of Quantum Information Sciences, Beijing 100193, China



(Received 31 July 2020; revised 1 September 2020; accepted 18 September 2020; published 29 September 2020)

Scanning tunneling microscopy and spectroscopy are utilized to study the atomic-scale structure and electronic properties of infinite-layer $\text{Sr}_{0.94}\text{La}_{0.06}\text{CuO}_{2+y}$ films prepared on SrRuO_3 -buffered $\text{SrTiO}_3(001)$ substrate by ozone-assisted molecular beam epitaxy. Incommensurate structural supermodulation with a period of 24.5 Å is identified on the CuO_2 -terminated surface, leading to characteristic stripes running along the 45° direction with respect to the Cu-O-Cu bonds. Spatially resolved tunneling spectra reveal substantial inhomogeneity on a nanometer-length scale and emergence of in-gap states at sufficient doping. Despite the Fermi level shifting up to 0.7 eV, the charge-transfer energy gap of the CuO_2 planes remains fundamentally unchanged at different doping levels. The occurrence of the CuO_2 superstructure is constrained in the surface region and its formation is found to link with oxygen intake that serves as the doping agent of holes in the epitaxial films.

DOI: [10.1103/PhysRevB.102.100508](https://doi.org/10.1103/PhysRevB.102.100508)

High-temperature superconductivity in cuprates emerges upon doping an antiferromagnetic Mott insulator due to strong electron correlations [1]. For understanding its mechanism and the emerging exotic phases (e.g., pseudogap and charge density waves) [2], a central issue that must be clarified is how the ground state of the Mott insulator in the CuO_2 planes evolves with doping. In theory, it was often hypothesized that the doping induces significant spectral weight transfer from the high- to the low-energy scale [3–5] so that the ground state changes dramatically and some extraordinary electronic states develop near Fermi level (E_F) [6]. This scenario has received some experimental support from both bulk- and surface-sensitive measurements [7–11], and attracted increasing interest in the community of strongly correlated electron physics [12]. However, the stability of the Zhang-Rice singlet with doping up to $x = 0.3$ in $\text{La}_{2-x}\text{Sr}_x\text{CuO}_4$ poses a challenge to the prevailing view of spectral weight transfer [13]. The doping resulted changes in the electronic structure of the CuO_2 planes remain elusive in cuprates.

Structurally, all cuprates consist of alternating CuO_2 and various charge reservoir layers along the crystallographic c axis [14]. Superconductivity occurs in the CuO_2 planes when the chemical doping is implemented in the adjacent nonsuperconducting charge reservoir layers. In order to understand the physics of the superconducting CuO_2 planes and thus the pairing mechanism, it is highly tempting to investigate directly the CuO_2 planes in experiment [15–18], provided the

structural elegance and complexity of the cuprate superconductors. Indeed, direct measurement by scanning tunneling microscopy (STM) on the CuO_2 planes of infinite-layer $\text{Sr}_{1-x}(\text{La}, \text{Nd})_x\text{CuO}_{2+y}$ films revealed a robust Mott-Hubbard band structure of CuO_2 against chemical doping [19], which is in contrast to the usual assumption mentioned above. In this study, we investigate the hole-doped CuO_2 planes in a wide doping region by preparing epitaxial $\text{Sr}_{0.94}\text{La}_{0.06}\text{CuO}_{2+y}$ (SLCO) films on SrTiO_3 (STO) substrate with a SrRuO_3 (SRO) buffer layer, aiming to establish a comprehensive picture about the evolution of the ground state of the CuO_2 planes versus doping.

The experiments were conducted on a commercial ultra-high vacuum (UHV) STM apparatus (Unisoku), which is connected to ozone-assisted molecular beam epitaxy (MBE) for *in situ* sample preparation. To reduce the lattice mismatch (1.2%) between SLCO and STO, a buffer layer of 70-nm-thick SRO films that has a pseudocubic lattice constant of 3.93 Å, comparable to that (3.95 Å) of SLCO, was firstly grown on Nb-doped STO(001) substrates using pulsed laser deposition technique. After being transferred into UHV, the SRO-covered substrates were annealed at 500 °C under ozone atmosphere to recover the atomically clean surface. The SLCO films were prepared by codeposition of high-purity metals (Sr, La, and Cu) from standard Knudsen cells under an ozone atmosphere of 1.1×10^{-5} Torr, as detailed elsewhere [19]. Prior to STM measurements at 78 K, polycrystalline PtIr tips were calibrated on MBE-grown Ag/Si(111) epitaxial films. Tunneling spectra were measured using a standard lock-in technique with a small bias modulation at 931 Hz.

*clsong07@mail.tsinghua.edu.cn

†xucunma@mail.tsinghua.edu.cn

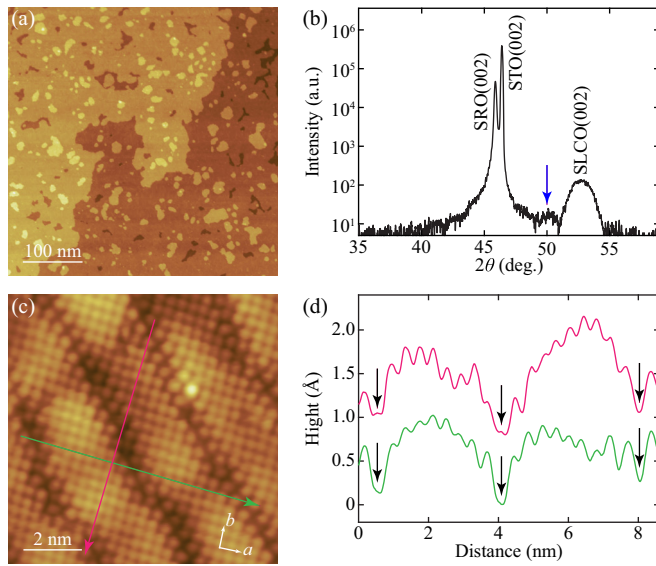


FIG. 1. (a) STM topography of SLCO epitaxial film (450 nm \times 450 nm, $V = -3.5$ V, $I = 20$ pA), decorated by small single-unit-cell islands. (b) XRD pattern around the SLCO(002) diffraction peaks measured using a monochromatic $CK\alpha 1$ radiation with a wavelength of 1.5406 Å. (c) Atomic-resolved STM topographic image of superstructural CuO_2 (9.2 nm \times 9.2 nm, $V = -0.85$ V, $I = 30$ pA). The bright spots correspond to the Cu atoms in the top layer. (d) Topographic profiles along the two Cu-O-Cu bond directions (a and b), color coded to match the arrowed lines in (c). Black arrows mark the positions of the invisible Cu atoms.

Figure 1(a) shows a large-scale STM topographic image of an as-prepared SLCO thin film with a thickness of 15 unit cells, in which the atomically flat nature of the surface is apparent. The steps have a height of approximately 3.6 Å, as expected for the infinite-layer SLCO and are further supported by *ex situ* x-ray diffraction (XRD) measurement in Fig. 1(b). In addition to the (002) diffraction peaks of STO and SRO, electron-doped SLCO phase occurs predominantly with a c -axis lattice constant of 3.47 Å. Meanwhile, a prominent new phase with a c -axis lattice constant of 3.6 Å (marked by a blue arrow) appears and the phase turns out to be hole-doped SLCO near the sample surface, which will be discussed in detail below.

Illustrated in Fig. 1(c) is an atomically resolved STM topography of SLCO surface with an in-plane lattice parameter of 3.9 ± 0.1 Å. Intriguingly, an incommensurate superstructure with a period of approximately 24.5 Å is observed, which runs along the diagonal direction of the CuO_2 square lattice and is very different from the primitive $\text{CuO}_2(1 \times 1)$ and reconstructed $\text{CuO}_2(2 \times 2)$ surfaces of the infinite-layer SLCO films on STO [19]. The superstructural CuO_2 planes are reminiscent of the well-known supermodulated BiO surfaces of Bi-family cuprates [15,17,18,20]. The superstructure can be more clearly seen by line profiles along a and b axes in Fig. 1(d), where the black arrows denote the invisible atom rows along the $[1\bar{1}0]$ direction. Such observation that the atoms in every eight or nine Cu atoms are invisible to STM is usually caused by structural displacement [21,22], similar to

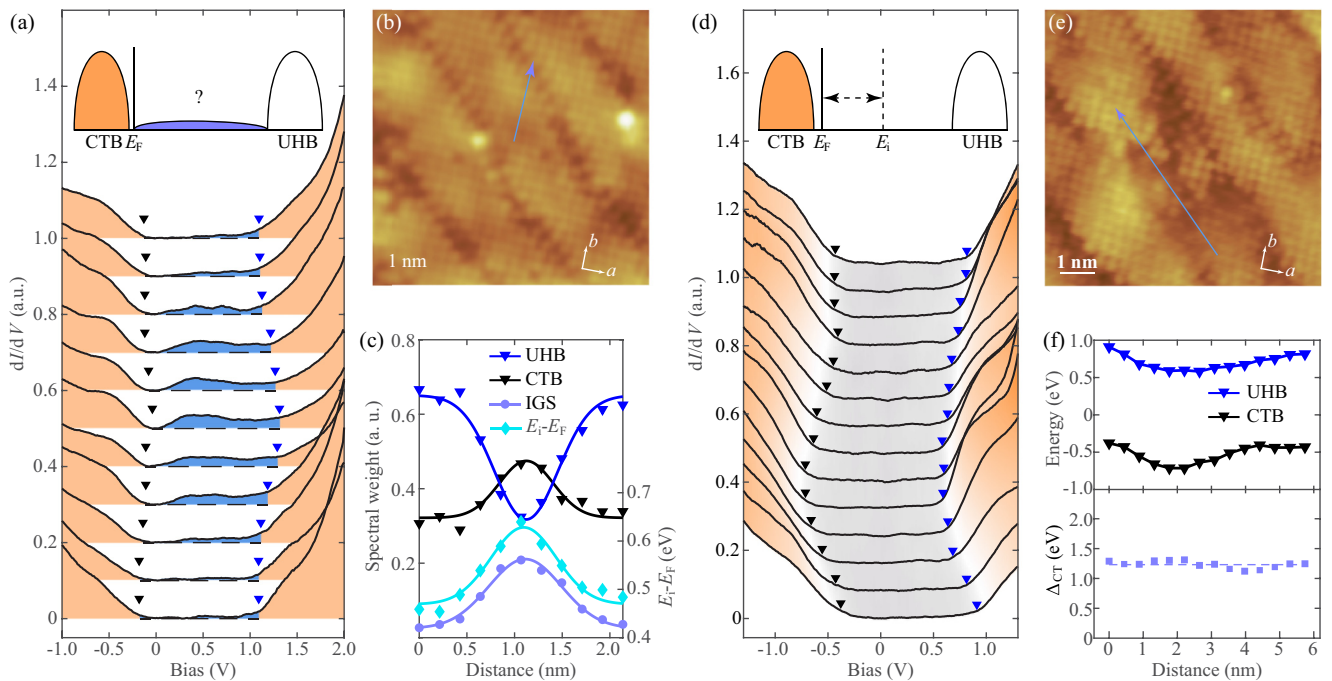


FIG. 2. (a) Spatially resolved tunneling conductance dI/dV spectra (setpoints: $V = -1.5$ V, $I = 200$ pA) acquired along the blue arrow in (b). Black and blue triangles mark the onset energies of CTB and UHB, respectively. Color-shaded areas measure spectral weights of CTB (left), IGS (middle), and UHB (right), respectively. Inset illustrates the schematic band structure of doped CuO_2 . (b) STM topography of as-prepared SLCO (9.7 nm \times 9.7 nm, $V = -1.2$ V, $I = 10$ pA). (c) Space-dependent variations in spectral weights and E_F shift relative to E_i . (d) Spatially resolved dI/dV spectra (setpoints: $V = -1.5$ V, $I = 200$ pA) acquired along the blue arrow in (e). Black and blue triangles mark the onset energies of CTB and UHB, respectively. (e) STM topography (9.7 nm \times 9.7 nm, $V = -0.8$ V, $I = 10$ pA) of UHV-annealed SLCO films at 510°C for 1 h. (f) Space-dependent onset energies of UHB, CTB (top panel), and Δ_{CT} (bottom panel) in (d).

the Bi-family cuprate superconductors [23,24]. The structural supermodulation on the CuO_2 planes constitutes one of the main observations of this study.

Next, we characterize the electronic structure of this observed superstructural CuO_2 surface by measuring a series of dI/dV conductance spectra along a trajectory of 24.2 Å that almost covers the whole modulation period. The result is summarized in Fig. 2(a) and the corresponding surface is shown in Fig. 2(b). Evidently, all spectra are characterized by a charge-transfer gap (CTG) between two upturns in the density of the states. The two upturns correspond to the occupied charge transfer band (CTB) and the empty upper Hubbard band (UHB), respectively. The Fermi energy E_F ($V = 0$) is all close to the CTB, a hallmark of hole doping [19]. Given that the substitution of trivalent La^{3+} ions for Sr^{2+} contributes to electron carriers, this unexpected finding implies that oxygen intake acts as a doping agent for holes in SLCO explored here. In contrast to the p -type SLCO films at $x > 0.1$ [19], the (2×2) superstructure caused by an appreciable intake and periodic occupation of apical oxygen atoms is absent in Fig. 2(b). This indicates a relatively lower oxygen doping, reconciling with our observation that E_F is always located at an energy above CTB [Fig. 2(a)]. Furthermore, the spectra exhibit an obvious spatial inhomogeneity, as seen by the emergent in-gap states (IGS; blue shaded areas) within CTG. The IGS become more prominent in the bright regions in Fig. 2(b).

The spatial inhomogeneity becomes more evident when the spatial-dependent spectral weights of CTB, IGS, and UHB are deduced as the color-shaded areas in Fig. 2(a). We show in Fig. 2(c) that the spectral weight of CTB, being in phase with that of IGS, increases with reducing UHB weight. Such a result seems understandable in the context of the scenario that spectral weight of CTB and IGS at lower energy builds up from a transfer from that of UHB at higher energy upon hole doping [3–11]. However, extreme caution should be taken, because the magnitude Δ_{CT} of CTG remains unchanged and there exists a systematic E_F shift for different local doping [19], albeit small in the heavily doped case [see the cyan diamonds in Fig. 2(c)]. Given the fixed energy range during spectroscopic measurement, the hole-doping-induced E_F downward shifting would naturally yield an inverse correlation between the space-dependent spectral weights of CTB and UHB in Fig. 2(c). In addition, heavier hole doping often means more IGS, thereby leading to a positive relationship between the local IGS and CTB.

To provide further insight into the origin of hole doping and IGS, we annealed the samples under UHV condition. Figure 2(d) represents the tunneling spectra along a trajectory of 52.1 Å on the surface of the annealed SLCO sample shown in Fig. 2(e). While the UHV annealing reduces the oxygen intake and shifts E_F upwards [25], the electronic inhomogeneity becomes even more prominent: the brighter the STM contrast, the smaller the energy separation between E_F and CTB. Similar to the previous report [19], we determine the onset energies of CTB and UHB, as well as the separation Δ_{CT} between them [Fig. 2(f)] and find that CTB and UHB change in a synchronous manner so that Δ_{CT} remains essentially unchanged.

We also note the significant suppression of IGS after UHV annealing, and ascribe it to the reduction of doping level.

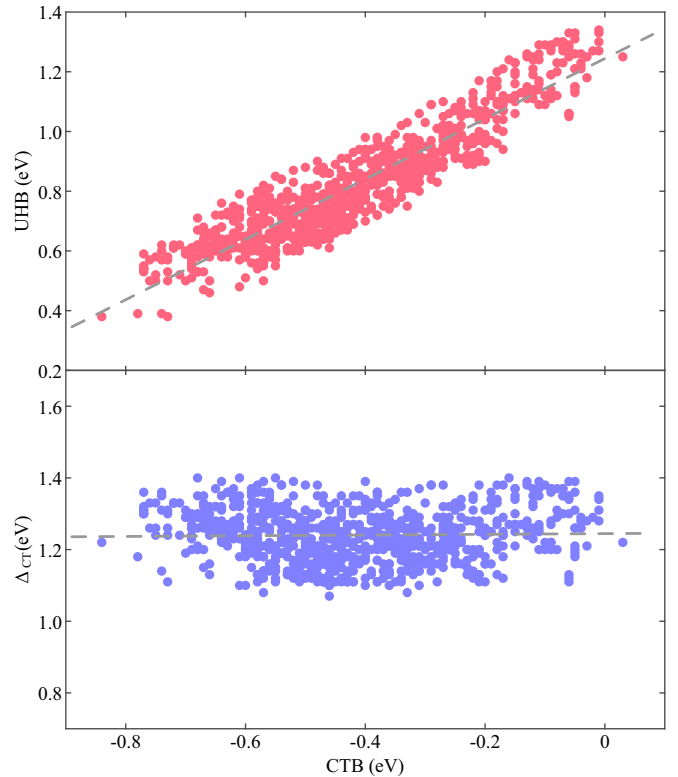


FIG. 3. Onset energy of UHB (red circles) and Δ_{CT} (blue circles) plotted as a function of CTB onset energy. The statistics involve more than 780 dI/dV spectra at varied positions and samples. Gray dashed lines show the best linear fits to the data.

Thus, the underlying cause of spatial inhomogeneity and emergent IGS is obvious: it is the inhomogeneous distribution of local dopants (oxygen and La atoms), and this doping inhomogeneity becomes more prominent after the UHV annealing. For increased doping of oxygen, E_F gradually moves from the midgap energy E_i (where the hole doping by oxygen compensates for the electron doping by La^{3+}) to the CTB, whereas the fundamental Mott-Hubbard band structure remains intact. As the dopants are densely populated to a critical concentration, probably relating to the Bohr radius of the dopant atoms in question [26,27], pronounced IGS or evanescent states emerge, prompting a transition from the Mott insulator to metallic or superconducting states. This bears a great similarity to the doping of semiconductors [28]. In any case, the fundamental Mott-Hubbard band structure of CuO_2 remains essentially unchanged, a hallmark of the self-modulation doping scheme [19].

The robustness of the Mott-Hubbard band structure against doping is further corroborated by annealing the SLCO films at different duration and measuring the corresponding conductance spectra in various regions. Figure 3 presents the extracted onset energies of UHB and Δ_{CT} as a function of the CTB onset energy. Compared to the CTB onset near E_F on the as-grown SLCO film, the local CTB, or equivalently E_F , can shift continuously by 0.7 eV after UHV annealing. Surprisingly, the onset energy of UHB scales linearly with that of CTB, yielding a slope of 1.01, very close to unity. Consequently, the Δ_{CT} remains almost the same for all

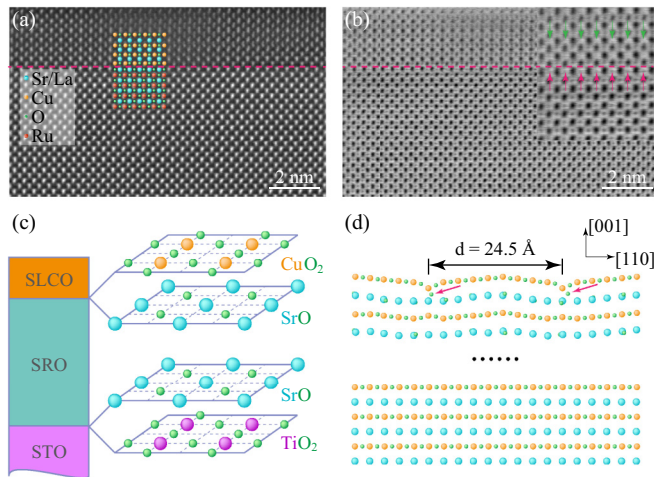


FIG. 4. (a) HAADF-STEM image across the interface between SLCO and SRO along the [001] axis, marked by the dashed line. (b) ABF-STEM image in the same field of view as (a). Inset shows a zoom-in of the SLCO/SRO interface. The magenta arrows mark the oxygen in the SrO layer of SRO, while the blue arrows indicate no apical oxygen in the Sr/La layers of SLCO. (c) Schematic structure of superstructural SLCO films prepared on SRO-buffered STO substrates, with the interfacial stacking of SLCO/SRO and SRO/STO magnified. (d) Possible diagram of the superstructural SLCO near the surface. The magenta arrows mark the incorporated oxygens that serve as the doping agent of holes.

spectra we studied (bottom panel of Fig. 3). The mean value of $\Delta_{CT} = 1.24 \pm 0.07$ eV turns out to be slightly smaller than that of SLCO films on STO substrates [19]. This might be caused by the reduced Madelung potential [29,30], probably owing to the slightly expanded in-plane lattice constant or the presence of structural supermodulation in the SLCO films on SRO. Nevertheless, the present study provides convincing experimental evidence that the doping changes little the fundamental Mott-Hubbard band structure of CuO_2 ; rather, it only induces a systematic shifting of E_F and IGS within CTG, as reported in n -type infinite layer [19].

Finally, we show by high-resolution scanning transmission electron microscopy (STEM) that the observed structural supermodulation occurs only in the surface regions of SLCO films. Figures 4(a) and 4(b) present the STEM images across the interface between the SLCO and SRO layer, taken in the high-angle annular dark-field (HAADF) and annular bright-field (ABF) modes, respectively. Evidently, the interface has a stacking sequence of $\text{RuO}_2\text{-SrO-CuO}_2\text{-Sr(La)}$, as schematically drawn in Fig. 4(c). This is quite distinct from the $\text{SrO-TiO}_2\text{-Sr(La)-CuO}_2$ stacking for SLCO films grown directly on the STO substrates [19]. No structural supermodulation and apical oxygen atoms are observed in the bulk of the epitaxial SLCO films, in contrast to the Bi-family cuprates [31]. Actually, the bulk phase belongs to the well-established n -type SLCO [19] and contributes to the pronounced n -SLCO(002) diffraction peak seen in Fig. 1(b). Taken altogether, our results suggest that the superstructure should develop solely near the top surface region, as schematically illustrated in Fig. 4(d). The structural supermodulation forms to accommodate incorporation of oxygen atoms [32], which slightly expands the c -axis lattice constant, as we observe above.

In summary, our detailed STM investigation of a novel superstructured CuO_2 plane has provided information about the doping of cuprate superconductors. The unchanged Mott-Hubbard band structure and systematic shift of E_F , which is consistent with the self-modulation doping scheme, turn out to be the two primary features of the doping on CuO_2 planes, irrespective of the spatial electronic inhomogeneity and the varied doping levels. Such a simple scheme may be applicable to a number of other strongly correlated materials.

We acknowledge P. Yu and Y. Lyu for providing the high-quality SRO/STO substrates. This work is financially supported by the Ministry of Science and Technology of China, the National Natural Science Foundation of China, and in part by the Beijing Advanced Innovation Center for Future Chip (ICFC).

- [1] P. A. Lee, N. Nagaosa, and X. G. Wen, *Rev. Mod. Phys.* **78**, 17 (2006).
- [2] B. Keimer, S. Kivelson, M. Norman, S. Uchida, and J. Zaanen, *Nature (London)* **518**, 179 (2015).
- [3] H. Eskes, M. B. J. Meinders, and G. A. Sawatzky, *Phys. Rev. Lett.* **67**, 1035 (1991).
- [4] M. B. J. Meinders, H. Eskes, and G. A. Sawatzky, *Phys. Rev. B* **48**, 3916 (1993).
- [5] D. S en echal, D. Perez, and M. Pioro-Ladri ere, *Phys. Rev. Lett.* **84**, 522 (2000).
- [6] P. Phillips, *Rev. Mod. Phys.* **82**, 1719 (2010).
- [7] S. Uchida, T. Ido, H. Takagi, T. Arima, Y. Tokura, and S. Tajima, *Phys. Rev. B* **43**, 7942 (1991).
- [8] M. A. van Veenendaal, G. A. Sawatzky, and W. A. Groen, *Phys. Rev. B* **49**, 1407 (1994).
- [9] N. P. Armitage, F. Ronning, D. H. Lu, C. Kim, A. Damascelli, K. M. Shen, D. L. Feng, H. Eisaki, Z.-X. Shen, P. K. Mang, N. Kaneko, M. Greven, Y. Onose, Y. Taguchi, and Y. Tokura, *Phys. Rev. Lett.* **88**, 257001 (2002).
- [10] C. Ye, P. Cai, R. Yu, X. Zhou, W. Ruan, Q. Liu, C. Jin, and Y. Wang, *Nat. Commun.* **4**, 1365 (2013).
- [11] P. Cai, W. Ruan, Y. Y. Peng, C. Ye, X. T. Li, Z. Q. Hao, X. J. Zhou, D. H. Lee, and Y. Y. Wang, *Nat. Phys.* **12**, 1047 (2016).
- [12] Y. Okada, D. Walkup, H. Lin, C. Dhital, T.-R. Chang, S. Khadka, W. Zhou, H.-T. Jeng, M. Paranjape, A. Bansil *et al.*, *Nat. Mater.* **12**, 707 (2013).
- [13] N. B. Brookes, G. Ghiringhelli, A.-M. Charvet, A. Fujimori, T. Kakeshita, H. Eisaki, S. Uchida, and T. Mizokawa, *Phys. Rev. Lett.* **115**, 027002 (2015).
- [14] C. Park and R. L. Snyder, *J. Am. Ceram. Soc.* **78**, 3171 (1995).
- [15] S. Misra, S. Oh, D. J. Hornbaker, T. DiLuccio, J. N. Eckstein, and A. Yazdani, *Phys. Rev. Lett.* **89**, 087002 (2002).

- [16] J. W. Harter, L. Maritato, D. E. Shai, E. J. Monkman, Y. Nie, D. G. Schlom, and K. M. Shen, *Phys. Rev. Lett.* **109**, 267001 (2012).
- [17] Y. F. Lv, W. L. Wang, J. P. Peng, H. Ding, Y. Wang, L. Wang, K. He, S. H. Ji, R. Zhong, J. Schneeloch, G. D. Gu, C. L. Song, X. C. Ma, and Q. K. Xue, *Phys. Rev. Lett.* **115**, 237002 (2015).
- [18] Y. Zhong, Y. Wang, S. Han, Y. F. Lv, W. L. Wang, D. Zhang, H. Ding, Y. M. Zhang, L. Wang, K. He, R. D. Zhong, J. A. Schneeloch, G. D. Gu, C. L. Song, X. C. Ma, and Q. K. Xue, *Sci. Bull.* **61**, 1239 (2016).
- [19] Y. Zhong, J.-Q. Fan, R.-F. Wang, S. Z. Wang, X. Zhang, Y. Zhu, Z. Dou, X.-Q. Yu, Y. Wang, D. Zhang, J. Zhu, C.-L. Song, X.-C. Ma, and Q.-K. Xue, *Phys. Rev. Lett.* **125**, 077002 (2020).
- [20] Ø. Fischer, M. Kugler, I. Maggio-Aprile, C. Berthod, and C. Renner, *Rev. Mod. Phys.* **79**, 353 (2007).
- [21] A. Inoue, H. Mukaida, M. Nakao, and R. Yoshizaki, *Physica C* **233**, 49 (1994).
- [22] F. Massee, Y. K. Huang, and M. Aprili, *Science* **367**, 68 (2020).
- [23] L. Shan, A. Ejov, A. Volodin, V. Moshchalkov, H. Wen, and C. Lin, *Europhys. Lett.* **61**, 681 (2003).
- [24] C. Zou, Z. Hao, H. Li, X. Li, S. Ye, L. Yu, C. Lin, and Y. Wang, *Phys. Rev. Lett.* **124**, 047003 (2020).
- [25] Y.-G. Zhong, J.-Y. Guan, X. Shi, J. Zhao, Z.-C. Rao, C.-Y. Tang, H.-J. Liu, Z. Y. Weng, Z. Q. Wang, G. D. Gu, T. Qian, Y.-J. Sun, and H. Ding, *Phys. Rev. B* **98**, 140507(R) (2018).
- [26] M. Alexander and D. F. Holcomb, *Rev. Mod. Phys.* **40**, 815 (1968).
- [27] P. P. Edwards and M. J. Sienko, *Phys. Rev. B* **17**, 2575 (1978).
- [28] P. Van Mieghem, *Rev. Mod. Phys.* **64**, 755 (1992).
- [29] A. Tsukada, H. Shibata, M. Noda, H. Yamamoto, and M. Naito, *Phys. C (Amsterdam, Neth.)* **445**, 94 (2006).
- [30] Y. Ohta, T. Tohyama, and S. Maekawa, *Phys. C (Amsterdam, Neth.)* **185**, 1721 (1991).
- [31] D. S. Song, X. F. Zhang, C. S. Lian, H. Liu, I. Alexandrou, I. Lazić, E. G. Bosch, D. Zhang, L. Wang, R. Yu, Z. Y. Cheng, C. L. Song, X. C. Ma, W. H. Duan, Q. K. Xue, and Z. Jing, *Adv. Funct. Mater.* **29**, 1903843 (2019).
- [32] Y.-F. Lv, W.-L. Wang, H. Ding, Y. Wang, Y. Ding, R. Zhong, J. Schneeloch, G. D. Gu, L. Wang, K. He, S.-H. Ji, L. Zhao, X.-J. Zhou, C.-L. Song, X.-C. Ma, and Q.-K. Xue, *Phys. Rev. B* **93**, 140504(R) (2016).